Hydrogenation of bio-oil into higher alcohols over Ru/Fe_3O_4-SiO_2 catalysts

Nikolay Cherkasov[1], Vishal Jadvani[1], Joshua Mann[2], Yaroslav B. Losovyj[2], Zinaida B. Shifrina[3], Lyudmila M. Bronstein[2,3,4], Evgeny V. Rebrov[1,5*]

1 School of Engineering, University of Warwick, Coventry, CV4 7AL, UK

2 Indiana University, Department of Chemistry, Bloomington, IN 47405, USA

3 A.N. Nesmeyanov Institute of Organoelement Compounds, Russian Academy of Sciences, 28 Vavilov St., Moscow, 119991 Russia

4 King Abdulaziz University, Faculty of Science, Department of Physics, Jeddah, Saudi Arabia

5 Tver State Technical University, Department of Biotechnology and Chemistry, 22 A. Nikitina St, 170026, Tver, Russia

* corresponding author: e.rebrov@warwick.ac.uk

Abstract

Liquid-phase hydrogenation of a solution of furfural, phenol and acetic acid has been studied in the 50-235 ^oC range over magnetic Ru/Fe_3O_4-SiO_2 catalyst targeting the renewable production of second generation biofuels with minimum hydrogen consumption. Phenol was fully hydrogenated to cyclohexanol in the entire temperature range. Below 150 ^oC, furfural was mainly hydrogenated to tetrahydrofurfuryl alcohol while hydrogenolysis to cyclopentanol was the main reaction pathway above 200 ^oC. The hydrogenation rate was doubled in an acidic solution (pH=3) as compared to that at a pH 6. The spent catalyst was regenerated and reused in subsequent catalytic runs.

Keywords: hydrogenation, magnetic recovery, Ru, pyrolysis oil

1. Introduction

Rising energy prices along with the depletion of fossil resources constitute one of the most important challenges of the modern world. To address the challenge, sustainable sources of energy, and in particular, fuels are required with the most promising source being biomass. There are several methods for fuel production from biomass such as conversion into syngas followed by synthesis of methanol, higher alcohols or hydrocarbons via the Fischer-Tropsch or methanol to gasoline processes [1,2]. A more targeted approach requires the growth of particular energy-rich organisms such as algae and their direct conversion into target fuels [3,4]. However, these processes require either long synthetic sequences or provide utilisation only of a very narrow range of biomass sources.

Fast pyrolysis is a particularly promising approach being simple and universal for various biomass sources. It occurs at moderate temperatures (480–520 °C), produces liquid oil product (convenient to handle) with yields up to 70 wt.% (of dry feed basis), and holds the potential to supplement crude oil as a liquid hydrocarbon feedstock. However, raw bio-oil has a number of drawbacks such as (i) low heating value, (ii) incompatibility with conventional fuels due to high oxygen content, (iii) high solids content, (iv) high viscosity, and (v) chemical instability [5–9]. Because of these, bio-oil cannot be used as a liquid fuel in internal combustion engines.

Bio-oil is usually upgraded via hydrodeoxygenation, cracking, steam reforming or other methods to overcome the problems [10–13]. Hydrodeoxygenation is considered to be a promising route for converting bio-oils to a traditional refinery-ready hydrocarbon feedstock. Given the multitude of C–O bond types in bio-oil, each with varying bond strength and thermodynamically preferred deoxygenation pathway, the term hydrodeoxygenation represents a complex network of many reactions. The process can be simplified by distinguishing reactions according to the hydrocarbon and oxygen elimination products using some model compounds present in the oil to understand the basic processes [14,15]. These studies are especially useful for comparison of the catalyst performance and essential for understanding of the reaction mechanisms and kinetics.

Phenol derivatives comprise up to 30 wt % of bio-oil [16]; therefore, phenol is widely used as a model molecule to study its hydrogenation or deoxygenation pathways [17]. A recent work was focussed on the hydrogenation of phenol in the aqueous phase through which the

use of an organic solvent could be eliminated by its replacement with water identified as a ‘green’ solvent [18,19]. The analysis can then be extended further, for example, acetic or propionic acid can be co-fed with a phenolic model compound to investigate reactant interactions before feeding the whole bio-oil [14,20,21]. In the hydrogenation of acetic acid, it was found that a Ru/C catalyst showed the highest activity, followed by Ru/Al_2O_3, Pt/C, Pt/Al_2O_3, Pd/Al_2O_3, and Pd/C [21]. Furfural and its derivatives are another main class of molecules present in bio-oil in the amounts up to 30-40 wt% [8,13,16]. Its hydrogenation was extensively studied in literature. Nakagawa et al. [22] demonstrated that introduction of Ir into Pd nanoparticles increases TOF due to increased adsorption of C=O bond. Pang et al. [23,24] showed an increased aldehyde hydrogenation and hydrodeoxygenation selectivity with the introduction of thiols over Cu-based catalysts. O’Driscoll et al. [25] demonstrated an excellent selectivity towards furfuryl alcohol over Pt-Sn catalysts in a range of solvents. Xu et al. [26] investigated the effect of additives such as acetone or acetic acid on the hydrogenation of furfural over Ni Raney catalysts. They found that both selectivity and activity can be changed dramatically due to different adsorption modes of substrate molecules over the catalyst surface.

Supported noble metals are attractive because they are known to activate hydrogen and are less susceptible to deactivation by water. Thus, they hold the potential to exhibit suitable performance with longer catalyst lifetimes. A recent report by Wildschut et al. highlights the promising activity of supported Ru, Pd, and Pt catalysts compared to traditional transition metal sulphide catalysts for the bio-oil hydrotreatment [27]. Model compounds have been used to develop an understanding of the role and interaction of the metal, promoter, support, and process conditions in deoxygenation.

Heeres et al. performed fundamental studies on hydrotreatment of bio-oils and model compounds using a Ru/C catalyst [28]. Different levels of upgrading were studied from stabilisation with low levels of oxygen removal through mild hydrotreatment to two-stage hydrotreatment with substantial oxygen removal. Lercher proposed a “one-pot” approach which is based on aqueous phase hydrodeoxygenation of phenolic monomers using bifunctional catalysis that couples precious metal catalysed hydrogenation and acid-catalysed hydrolysis and dehydration [29]. A more complex process involving hydrotreatment, esterification and cracking in supercritical ethanol on supported palladium catalysts has been reported [30]. This work demonstrated a significant improvement in a

number of properties such as removal of aldehydes, a decomposition of macromolecules and a decrease in viscosity as well as an increased heating value.

However, traditional bio-oil hydrodeoxygenation requires high-pressure H_2 in large excess, which significantly increases the cost of upgrading [31]. Bridgwater has estimated that 62 kg of H_2 is required to deoxygenate one tonne of bio-oil [34]. Moreover, a large number of by-products such as methane is usually formed resulting in the liquid fuel yield of only about 25% [32]. Therefore, significant economy can be achieved via minimization of the amount of H_2 required for deoxygenation by targeting only the most problematic substances.

An additional challenge posed by bio-oil is catalyst recovery which is difficult to do via filtering due to high particulate content, high viscosity and instability of bio-oil. In this respect, magnetic recovery of the catalysts seems particularly promising [33]. Magnetic catalyst recovery generates more environmentally friendly processes, cheaper products, and conserved energy for a range of processes [34–37]. In the majority of cases, catalytic complexes or nanoparticles (NPs) are placed on the surface of magnetic NPs [33,38,39], but for efficient magnetic separation, the NP aggregation is required [40,41]. In addition, NP based catalysts are normally synthesized in microgram amounts making scaling up a difficult task. Composite materials consisting of magnetite NPs and silica received considerable attention as catalytic supports. Well-defined and monodisperse core-shell NPs with a magnetic core and silica shell can be prepared using a microemulsion approach [42], but again scaling up and fast magnetic separation are problematic. When SiO_2 filled with Fe_3O_4 NPs bearing catalytic species are prepared in one-pot procedure [43] or with subsequent addition of corresponding species [44], larger amounts of catalysts can be obtained and NPs are aggregated, allowing easy magnetic separation. However, some catalytic species could be buried within these aggregates.

Many researchers performed hydrogenation of model bio-oil components such as furan and derivatives of phenol [8,29,45–47]; however, far less attention have been devoted to the study of the hydrogenation of more complex mixtures. Recently, substantial solvent effects on hydrogenation rates were identified, which are expected to play a major role in bio-oil hydrogenation [48]. In the current work, we have studied hydrogenation of mock bio-oil containing three major components of the real oil such as phenol, furfural and acetic acid. The catalyst recycling which is essential for successful industrial applications is usually not performed, because recycling of conventional supported catalysts requires an aggressive

oxidative treatment which leads to deactivation via sintering. To avoid this problem, we used magnetically-recoverable Ru catalysts deposited on a composite Fe_3O_4-SiO_2 support.

2. Experimental Procedures

2.1. Materials

Ruthenium(III) acetylacetonate ($Ru(acac)_3$, 97 wt%), iron(III) nitrate (98 wt%), mesoporous silica gel 425 mesh, furfural (98 wt%), phenol (98 wt%), acetic acid (98 wt%) and calcium carbonate (99 wt %) were used as purchased from Sigma-Aldrich. Ethylene glycol (99 wt%) and tetrahydrofuran (THF, 99 wt%) were supplied by Macron Fine Chemicals. Ethanol (95 vol%) purchased from EMD was used without purification. Deionized water was used though the study.

2.2. Synthesis of Fe_3O_4-SiO_2

The Fe_3O_4-SiO_2 material was obtained using a procedure described in ref. [49]. The solution of $Fe(NO_3)_3$, 2 g in 10 mL of ethanol was prepared, mixed with 2.5 g of silica gel and left stirring overnight in air for solvent evaporation. The material obtained was dried at room temperature in a vacuum oven for 2 hours. Afterwards, approximately 0.2 mL ethylene glycol was added and mixed with a spatula. The Fe_3O_4-SiO_2 formation was carried out in a tube furnace at a temperature of 250 °C (heating rate of 2 °C min^{-1}) for 5 hours in a flow of argon.

2.3. Synthesis of Ru/Fe_3O_4-SiO_2

Impregnation of the magnetic support with Ru compound was performed by adding 0.5 g of Fe_3O_4-SiO_2 prepared in the previous step into a solution of 0.099 g of $Ru(acac)_3$ in 2.5 mL of tetrahydrofuran (THF). The solvent was evaporated by stirring in air overnight followed by drying for 2 h at room temperature in a vacuum oven. Ethylene glycol, 0.2 mL, was added to the powder which became red. Reduction and decomposition of Ru precursor were performed by placing the samples into a quartz tube furnace and heating at 2 °C min^{-1} under a flow of argon at 300 °C. Prior to the catalytic reaction, the catalyst was reduced at 300 °C in the flow of 10 mL min^{-1} (STP) 5 vol.% H_2/N_2 for 4 h, cooled to room temperature and passivated in the flow of 10 mL min^{-1} (STP) 1 vol. % O_2/N_2. The catalyst was stored in sealed vials under nitrogen atmosphere. Ru nominal loading was 5 wt.% and the catalyst was referred to as 5 wt.% Ru/Fe_3O_4-SiO_2. The reference 5 wt% Ru/SiO_2 catalyst was obtained in the same way skipping the introduction of the magnetic nanoparticles.

2.4. Catalytic activity measurements

Acetic acid (120 mg), furfural (180 mg, distilled before experiment) or phenol (180 mg) were dissolved in 25.0 mL of water. Then 10.0 mL of the solution was transferred into a 25 mL vessel and purged ten times with 5 bar H_2 to remove dissolved air. The catalyst (10-500 mg) was placed in a 160 mL high-pressure stainless steel reactor (Parr Instruments). The reactor was filled with water (100 mL) and flushed five times under stirring with N_2 (40 bar) to remove dissolved air. The reactor was heated to the desired temperature. Below 150 ^oC, the reaction mixture was fed into the reactor after it reached the desired temperature. At higher reaction temperatures the reaction mixture was fed into the reactor at 150 ^oC and the reactor was further heated under a hydrogen pressure of 1 bar till the desired temperature. On reaching the reaction temperature, the H_2 pressure was increased to 60 bar and kept constant, while the reaction timer was started and the reaction was performed for different time intervals (typically 60-240 min) at a stirring rate of 1200 rpm. After the reaction, the reactor was cooled and H_2 was replaced with N_2. The solution was decanted holding the catalyst with a 10 kg pull NdFeB magnet. The reference experiments of phenol hydrogenation were performed in the same manner but without the addition of furfural into the reaction mixture. To adjust the pH of the reaction mixture, a small amount of $CaCO_3$ was added on mixing and monitoring pH using a pH meter.

The liquid phase was analysed with a gas chromatograph (Shimadzu GC-2010) equipped with a 30 m 0.32 mm Stabilwax capillary column and an FID detector. An analysis procedure was optimized to ensure that no injector discrimination of heavy and reactive products occurred via a splitless injection with solvent focusing. In this procedure, about 1 mL of the reaction mixture was taken periodically through a 2 m, 0.15 mm i.d. stainless air-cooled capillary tube, discarding the first 0.4 mL. The solution taken (500 µL) was mixed with 200 µL of the solution of 2 internal standards (25 mM 2,6-dimethylphenol and 40 mM 1,3-dioxolane in 1,4-dioxane). Two internal standards were required for accurate analysis of low- and high-boiling compounds such as tetrahydrofuran and phenol, respectively. The amount of lighter products (b.p. < 100 ^oC) was always close to the detection level (below 0.1 mM). The gas phase was analysed by injecting gas samples into the mass-spectrometer at regular time intervals. The amounts of CH_4 and CO_2 were always below 1 vol.%. A carbon balance was better than 90 % for the experiments performed at the reaction temperatures below 200 ^oC and decreased to about 85 % at 235 ^oC, likely due to oligomerisation of furfural. A series of experiments with various stirring rates and catalyst

amounts confirmed the absence of mass transfer limitations in the whole range of experimental conditions studied.

2.5. Characterisation

Surface area and porosity data were obtained from liquid nitrogen adsorption measurements on an ASAP 2020 analyser from Micromeritics. The samples for high resolution transmission electron microscopy (HRTEM) were prepared by placing a drop of a sample suspension onto a carbon-coated Cu grid. HRTEM images were acquired on a JEOL 3200FS transmission electron microscope equipped with an Oxford Instruments INCA EDS system at an accelerating voltage of 300 kV. Images were analysed with the ImageJ software [50]. Phase composition was studied using X-ray powder diffraction (XRD) on an Empyrean from PANalytical instrument equipped with a Cu target (λ = 1.54 Å) at the step-size of 0.02 ^{o} 2θ.

The samples for X-ray photoelectron spectroscopy (XPS) were prepared by placing a droplet of the sample suspension in chloroform on a Si wafer. The measurements were conducted using a PHI Versa Probe II instrument equipped with a monochromatic Al Kα source. The X-ray beam size was about 100 μm, power of 25 W at an acceleration voltage of 15 kV. The calibration of the instrument work function was performed using a 84.0 eV binding energy (BE) Au 4f7/2 line for metallic gold. The dispersion was corrected using BEs of 284.8 eV, 932.7 eV and 368.3 eV for the C 1s line of aliphatic carbon present, Cu 2p3/2 and Ag 3d5/2 photoemission lines, respectively. The double charge compensation system was used on all samples. The instrumental resolution was calculated to be higher than 0.125 eV using the Fermi edge of the valence band for metallic silver. The spectra were recorded using a SmartSoft XPS software with an energy step of 0.1 eV.

Two sets of iron leaching experiments were performed: (i) in the stainless Parr autoclave under reaction conditions and (ii) glass vials at room temperature to avoid leaching of the autoclave material. The leaching test in the Parr reactor was performed placing 60 mf of the catalyst into the reactor and filing it with 110 mL of a solution of mock oil with the pH of 2.5, 4.5 and 6.5 the same way as during the reaction. The reaction mixture was flushed with N_2, H_2 and heated to 150 ^{o}C and cooled after 2 h. The catalyst was recovered by centrifuging, washed with water (2 x10 mL) and dried at 70 ^{o}C. Then 10.0 mg of the catalyst was placed in a volumetric flasks, and left with 1 mL of aqua regia under sonication to extract iron

turning black catalyst into transparent silica powder. The solution was diluted 1000-fold and analysed using a PerkinElmer 5300DV ICP-OES spectrometer for Fe. The liquid phase after the reaction was also analysed.

Iron leaching in glass vials was performed using the catalysts as well as Fe_3O_4 or Fe_2O_3 powders (Sigma-Aldrich, 98 wt%) placed into glass vials. The pH of the aqueous solution of 0.1 g furfural, 0.1 g phenol and 1 g acetic acid in 50.0 mL water was adjusted with $CaCO_3$ till the value of 2.5, 4.5 and 6.5. The solutions, 10.0 mL, were placed with the studied materials into a convection oven and left for 48 h at 80 ^oC. The solutions obtained were filtered, diluted 100-fold with water and analysed using a PerkinElmer 5300DV ICP-OES spectrometer for Fe.

Chemisorption of CO was performed using a flow chemisorption methodology described in refs. [51,52]. The catalyst (100 mg) before the test was oxidised in a 30 vol.% O_2 in N_2 mixture at 350 ^oC for 30 min, then cooled to 50 ^oC in the flow of He followed by reduction in a 5 vol.% H_2 in N_2 mixture for 30 min at 300 ^oC. After the reduction step, the sample was cooled in a He flow (10 mL min^{-1} STP) to 30 ^oC and then the flow was switched to a mixture of CO (500 ppm) and Ar (400 ppm) in He. The concentrations of CO and Ar were monitored using a mass spectrometer. The Ar signal was used as internal standard to determine the exact reactor volume, while the CO signal was used to determine the total CO capacity of the material. The CO signal was calibrated using a 0.5 wt.% Pt/Al_2O_3 reference catalyst (from Micromeritics) with known adsorption capacity.

The temperature programmed oxidation study has been performed by placing 30 mg of the catalysts recovered after the reaction at 150 ^oC and 235 ^oC into a quartz tube connected to a series of mass-flow controllers and a quadrupole mass spectrometer. After flushing the sample with 10 mL min^{-1} of He for 10 min to stabilise determine the background signal of H_2O, CO and CO_2, the sample was heated at a rate of 5 ^oC min^{-1} till 550 ^oC in the flow of 0.6 mL min^{-1} O_2 and 10 mL min^{-1} He (STP). The concentration of CO_2 was calibrated by decomposition of a series of $PbCO_3$ samples (Sigma-Aldrich, 99 wt%).

3. Results and discussion

3.1. Hydrogenation pathways

The mock pyrolysis oil was composed as an aqueous solution of furfural, phenol and acetic acid. The corresponding hydrogenation pathways are presented in Figure 1. **Error! Reference source not found.**Phenol (PhOH) can be hydrogenated to cyclohexanol (C_6OH) via cyclohexanone (C_6O) obtained via an unstable cyclohexanol [53] intermediate. These reaction pathways are observed for many phenol derivatives [53–55]. Compared to phenol, which is unsuitable for transportation fuel applications due to its corrosive behaviour and a possibility to solidify, cyclohexanone and cyclohexanol may be acceptable fuels. They are non-corrosive liquids under standard conditions with the enthalpy of combustion (35.8 and 37.2 kJ g^{-1}, respectively) close to that of gasoline (~47 kJ g^{-1}). It is known that phenol derivatives can be converted into hydrocarbons in a highly acidic environment or over bifunctional (metal-acidic) catalysts [29,46], but these products were not observed under the conditions studied.

The other abundant components of bio-oil, furfural and furfuryl alcohol derivatives, polymerise over time, which may cause problems during storage or combustion in engines. Furfural can be hydrogenated via the aldehyde group or the aromatic ring. The initial hydrogenation step over noble metal catalysts is an aldehyde reduction followed by the reduction of the furan ring [22,24,25,56,57] as presented in Figure 1. Moreover, furfuryl alcohol can be hydrogenated into cyclopentanone almost quantitatively over Ru catalysts supported on acidic metal-organic frameworks [58]. The traditional supports such as carbon provide impregnated with noble metal catalysts provide a yield of 40-75% [59]. The proposed reaction mechanism includes the formation of 4-hydroxy-2-cyclopentenone as an intermediate [60]. At higher reaction temperatures (above 150-200 ^oC), the hydrogenolysis can take place resulting in deoxygenation or furan ring opening that results in the formation of aliphatic alcohols, diols [14,61–64].

For fuel applications, the unstable furfural derivatives should be hydrogenated into more stable derivatives such as tetrahydrofurfuryl alcohol (HFA) or cyclopentanone (C_5O). Comparing these two hydrogenation routes, the formation of HFA seems advantageous because of (i) higher standard enthalpy of combustion (-2.96 vs. -2.87 MJ mol^{-1} for HFA and C_5O, respectively) and (ii) the possibility of subsequent quick hydrogenation of C_5O into

cyclopentanol (C_5OH) which further increases hydrogen consumption. Acetic acid can be hydrogenated into ethanol and form esters, but literature data shows that this reaction proceeds at a noticeable rate only above 250 ^oC [14,65,66].

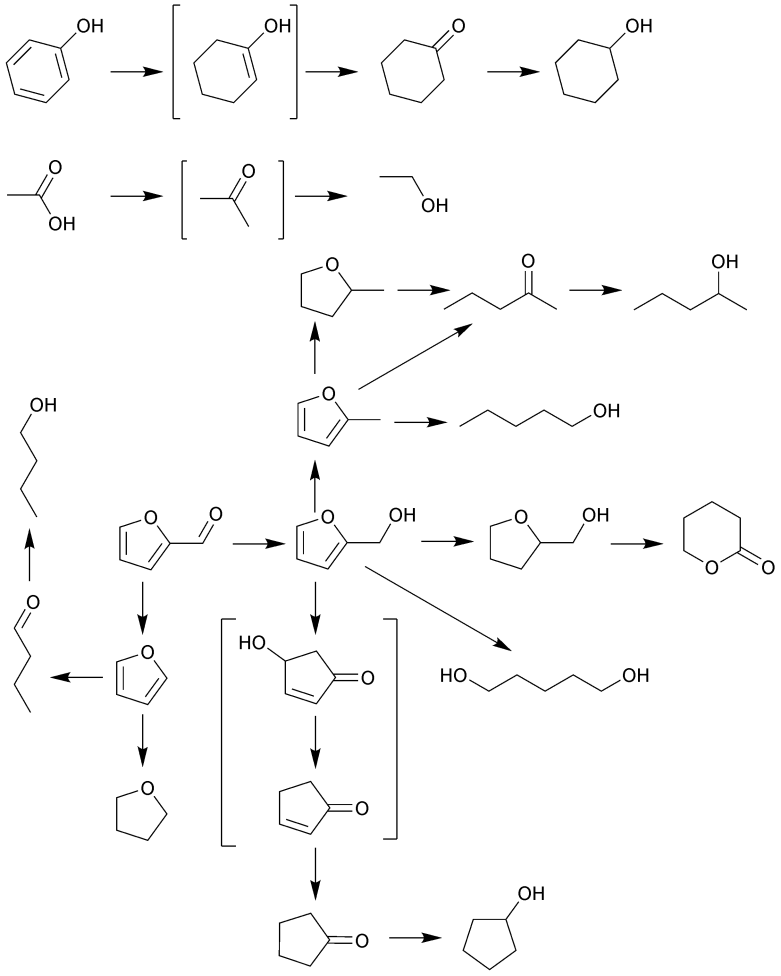

Figure 1. Hydrogenation reaction pathways for phenol, acetic acid, and *furfural with unstable intermediates presented in brackets.*

3.2. Catalyst characterization

X-ray diffraction data (Figure 2a) show phase composition of the catalyst which contains amorphous SiO_2, Ru NPs and Fe_3O_4. The main reflection at 43 two theta degrees, which corresponds to Ru nanoparticles, is overlapped by that of Fe_3O_4 as can be seen by comparing the patterns for Ru/Fe_3O_4-SiO_2 and the Fe_3O_4-SiO_2 support. Hence, deconvolution of the pattern has been performed to determine the width of the Ru reflection followed by using Scherrer's equation for estimation of the crystallite sizes of Ru (1.9 nm) and Fe_3O_4

(magnetite, 12 nm). The HRTEM study (Figure 2b) shows that both Ru and Fe_3O_4 nanoparticles (2.0±0.5 and 5.4±0.9 nm, respectively) are uniformly distributed in the silica support. It should be noted that Scherrer's equation can be considered only semi-quantitative for nanoparticles because a crystalline strain and size affect the width of the observed peaks. Considering this limitation, the results of both methods are in good agreement. Magnetic properties of the catalyst studied have been reported in ref. [37]. The results show superparamagnetic behaviour of the catalyst with a blocking temperature of -170 ^oC, which is typical for Fe_3O_4 nanoparticles of the observed size.

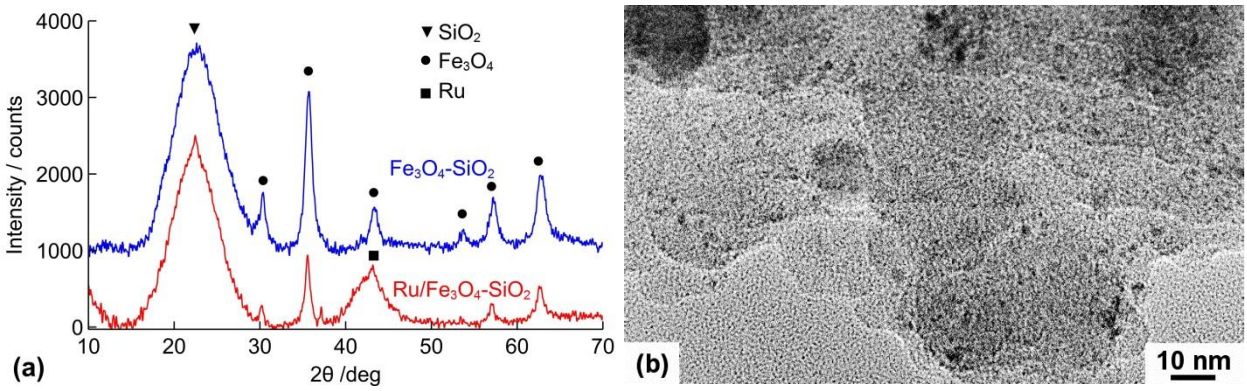

Figure 2. (a) XRD pattern and (b) HRTEM image of the 5 wt.% Ru/Fe_3O_4-SiO_2 catalyst.

The survey XPS (not presented) showed a Ru loading of 5.8 wt. %, which is higher than the nominal loading of 5.0 wt. %. A slightly higher than the nominal value is likely attributed to the formation of Ru nanoparticles on the outer surface of the support. As XPS is sensitive only to the very outer layer of the surface, the signal from bulk silica was likely not detected resulting in an overestimated Ru content. The high resolution (HR) XPS Ru3d spectrum is shown in **Error! Reference source not found.**Figure 3. The Ru(0) to Ru(IV) molar ratio was 1:1.38 in the as-synthesised catalyst. The Ru(IV) species are likely to be formed during surface oxidation in air in the last step of the catalyst preparation. Therefore, prior to the kinetic measurements, the catalyst was reduced in a flow of 5 vol.% H_2/N_2 at 300 ^oC to ensure that Ru was fully reduced to the metallic state.

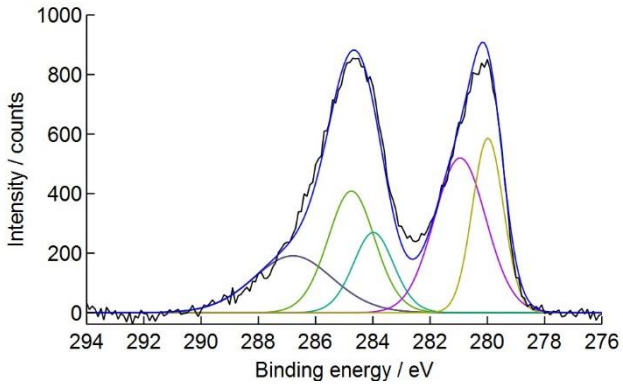

Figure 3. HR XPS Ru 3d of the 5 wt.% Ru/Fe_3O_4-SiO_2 catalyst.

The total CO chemisorption capacity of the catalyst was 25.9 μmol g^{-1} which corresponds to a Ru dispersion of 5.6 % assuming a 1:1 adsorption ratio of CO molecules on the Ru surface atoms. Appling the model of monodisperse fully accessible spherical particles, this value results in an expected mean Ru nanoparticle diameter of 16 nm which significantly exceeds the values obtained from both TEM (1.9 – 2.0 nm) and XRD. Therefore, it can be concluded that a significant fraction of Ru was not accessible to CO either because of surface blockage or close proximity to other Ru particles.

There are two possibilities for blocking the Ru surface: (i) residual organic impurities adsorbed on the surface obtained from, for example, $Ru(acac)_3$ decomposition or (ii) masking Ru by the Fe_3O_4 NP surface if the former is embedded in between the latter. The total CO chemisorption capacity of the catalyst after calcination in a 30 vol. % O_2/N_2 mixture at 550 ^oC only slightly decreased to 24.1 μmol g^{-1}. Therefore, it can be concluded that no blockage of active sites with residual organic molecules occurs in the as-synthesised catalysts. The possibility of Ru surface blockage by the support seemed unlikely because Ru nanoparticles were introduced at the latest stage, so the Ru precursor was unlikely to get into inaccessible positions. To check this hypothesis, a reference 5 wt.% Ru/SiO_2 catalyst was compared with the magnetically recoverable Ru/Fe_3O_4-SiO_2 catalyst. The total CO chemisorption capacity in the Ru/SiO_2 catalyst was 260 μmol g^{-1} corresponding to a Ru nanoparticle diameter of 1.6 nm, which was in good agreement with that determined by TEM (Figure 2). The initial phenol hydrogenation rate for the Ru/SiO_2 catalyst was 1.05 mmol g^{-1} s^{-1}, while that of the Ru/Fe_3O_4-SiO_2 catalyst was only 0.11 mmol g^{-1} s^{-1} which corresponded to the turnover frequencies (TOF) of 4.0 and 4.5 s^{-1}, respectively. Close TOF values indicate that the decrease in the reaction rates was caused by the surface blockage

rather than electronic interactions when the TOFs are expected to change. Hence, the presence of magnetic Fe_3O_4 particles does result in a significant decrease in the available surface area of Ru. The reason might be either proximity of Ru particles formed in the SiO_2 pores mostly filled with Fe_3O_4 NPs or surface masking of Ru NPs by Fe_3O_4 NPs. Despite this shortcoming, the Ru/Fe_3O_4-SiO_2 catalyst studied provides a representative example of a magnetically recoverable supported catalyst with an exposed magnetic NPs.

3.3. Effect of temperature on the product distribution

The effect of reaction temperature on the reaction rate and product distribution in the hydrogenation of mock oil is presented in Figure 4**Error! Reference source not found.**. The range of reaction products observed in the present work agrees well with earlier studies where furfural and phenol hydrogenations were performed separately [19,22,56–60,62,67]. The hydrogenation of phenol started only after the full conversion of furfural in the entire temperature range. This suggests that furfural has the highest heat of adsorption on the catalyst surface and blocks effectively all the Ru active sites preventing adsorption of phenol. Because of significant adsorption effects, it can be concluded that the reaction kinetics is described by a Langmuir-Hinshelwood model. A detailed kinetic modelling of the reaction pathways was attempted, but the presence of a large number of products made the determination of the rate and adsorption constants inaccurate.

Interestingly, Elliott and Hart, who performed hydrogenation of a mock oil containing 2-methoxyphenol, furfural and acetic acid (all 5 wt.%), found that phenolic and furan species are hydrogenated simultaneously, likely, because of much higher concentrations (~0.5 M) used in their study [14]. Similarly, the product distribution in their study was significantly wider and included diols. The latter are likely formed at much higher acidity of the solution containing 5 wt. % of acetic acid and a 3.5-fold catalyst loading of 2.5 g L^{-1} as compared to that in the present work. This resulted in much faster rates of hydrogenation, hydrogenolysis and hydrolysis reactions. The comparison with our data suggests that decreasing the concentration of individual components of the oil increases selectivity and results in lower hydrogen consumption per carbon atom present in the bio-oil.

The FA, C_5O and C_6O concentration profiles confirm that these are intermediate species, and their concentrations can be effectively adjusted with the reaction temperature. For example, a maximum selectivity of 83 % towards FA is obtained at 100 ^oC, while a

maximum selectivity of 80% towards C_5O is obtained at 235 ^oC. A high selectivity towards C_5O is likely caused by its quick desorption from the catalyst surface at a higher reaction temperature.

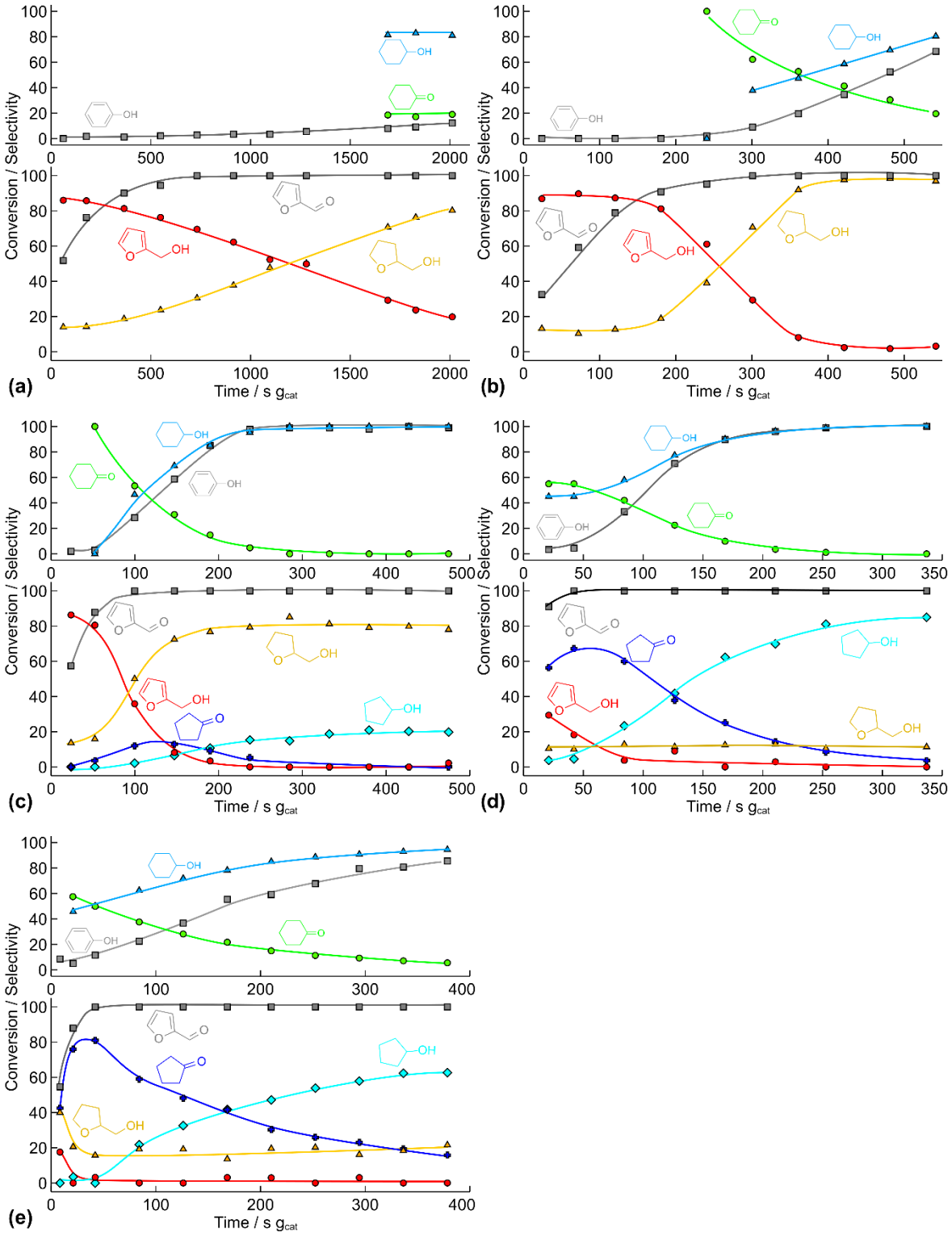

Figure 4. Product distribution in the hydrogenation of mock bio-oil (7 mM of phenol, 7 mM of furfural, 6 mM of acetic acid dissolved in 110 mL of water) under 60 bar H_2 pressure and a temperature of (a) 50 ºC, (b) 100 ºC, (c) 150 ºC, (d) 200 ºC, (e) 235 ºC. *Top plot: in phenol hydrogenation, (■) phenol conversion and selectivities towards (●) cyclohexanone and (▲) cyclohexanol. Bottom plot: in furfural hydrogenation, (■) furfural conversion and selectivities*

towards (●) furfuryl alcohol, (▲) tetrahydrofurfuryl alcohol, (+) cyclopentanone and (♦) cyclopentanol.

The reaction rate steadily increased as the temperature increased from 50 to 200 ^{o}C. However, the hydrogenation rate of phenol was significantly lower at 235 ^{o}C compared to the experiment performed at 200 ^{o}C. This phenomenon could be caused either by catalyst deactivation due to adsorption of heavy reaction products or decreased catalyst coverage with the reacting species. We have performed a TPO study to study for coke adsorption, which showed a considerably higher total amount of CO_2 released of 2.3 and 7.6 μmol mg^{-1} for the catalysts after the reaction at 150 and 235 ^{o}C, respectively. Moreover, Figure 5 shows a notable difference in the TPO profiles at the temperature above 400 ^{o}C. For the sample recovered after the reaction at 235 ^{o}C, there is a CO_2 evolution peak around 440 ^{o}C indicating the presence of heavy coke. These data indicate that the catalyst deactivation observed was caused by coke formation.

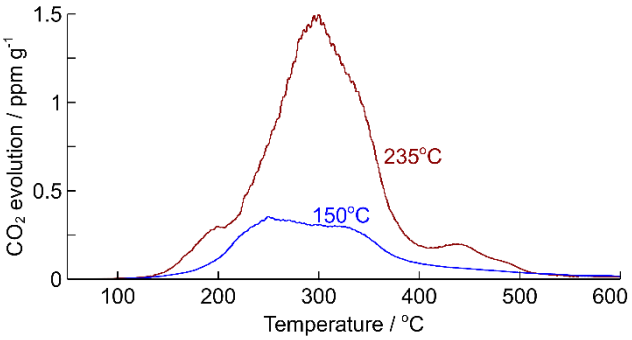

Figure 5. CO_2 evolution profiles obtained on oxidation of catalysts recovered after mock oil hydrogenation at 150 and 235 ^{o}C.

The preferential hydrogenation of furfural into C_5OH occurred at 150 ^{o}C. This temperature seems to be optimal for oil hydrogenation because phenol, as well as furfural, and furfuryl alcohol were preferentially hydrogenated into C_6OH and HFA, respectively, providing minimum hydrogen consumption and removal of corrosive and unstable compounds.

3.4. Effect of pH on the reaction rates

Catalyst recovery under the studied reaction conditions remains difficult because the exposed magnetic NPs may be dissolved in an acidic solution according to reaction (Eq. 1):

$$Fe_3O_4 + 6H^+ + H_2 \leftrightarrow 3\ Fe^{2+} + 4H_2O \qquad (1)$$

The equilibrium degree of iron dissolution under reaction conditions can be calculated using Eq. 2,

$$[Fe^{2+}] = \sqrt[3]{[H^+]^6\, p_{H2} \exp(2\ F\ E^o_{Fe3O4/Fe2+}\ R^{-1}\ T^{-1})} \qquad (2)$$

where $[Fe^{2+}]$ and $[H^+]$ are the concentrations of Fe^{2+} and H^+ in the solution, p_{H2} is the hydrogen pressure, $E^o_{Fe3O4/Fe2+}$ is the standard redox potential, *T* is the reaction temperature, and *F* and *R* are the Faraday and universal gas constants, respectively. The concentration of the Fe^{2+} species in equilibrium with Fe_3O_4 as a function of solution pH is shown in *Figure 6*. It demonstrates that a stable operation of the catalyst is possible at a pH value of above 4.5, while a full dissolution of the iron oxide support is expected at a pH below 4.0.

The experimental study of the dissolution phenomenon was also carried out. The catalysts as well as Fe_2O_3 and Fe_3O_4 samples were placed in glass vials and exposed to the reaction solutions of various pH for 48 h at 80 ^oC. However, a negligible (< 0.1%) leaching was observed, which was likely caused by slow dissolution rates under such conditions.

A set of experiments was performed in the batch reactor recovering the catalysts by centrifuging and analysing Fe level both in the catalyst and the solution. The results presented in *Figure 6* show good agreement with the calculated results. Similarly, the concentration of Fe in the solution was 45 ppm at the solution pH of 2.5 and below 0.3 ppm at higher pH values.

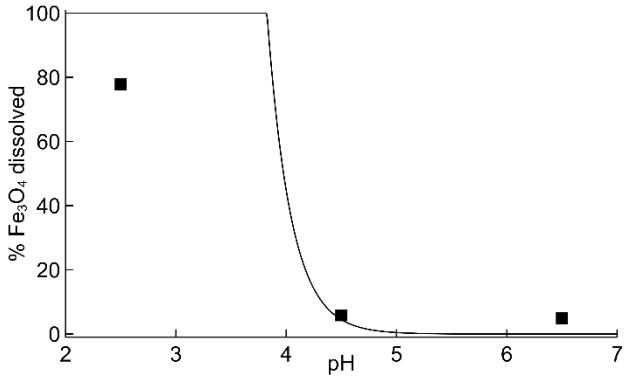

Figure 6. Calculated (solid line) and experimental (■) fraction of Fe_3O_4 dissolved from the 5 wt.% Ru/Fe_3O_4-SiO_2 catalyst in 100 mL of mock oil under the reaction conditions.

A solution of phenol has a pH value of about 5.5. Hence, high acidity of bio-oil is caused by the presence of carboxylic acids such as formic, acetic and propionic. The hydrogenation data show that acids cannot be hydrogenated under the conditions studied; therefore, the acids should either be separated or neutralised prior to the reaction to prevent catalyst dissolution. The acid separation can be performed using ion exchange resins without the water separation stage [8,16,68,69]. In this study, however, a simpler and more scalable approach was chosen – neutralisation with chalk ($CaCO_3$), which increased the pH of the reaction mixture from 3.0 to a final value of 6.0. Calcium acetate formed as a by-product of neutralization can be removed in the post-processing step of water separation from the oil using solvent extraction or via reaction mixture distillation.

The product distribution obtained in the hydrogenation of neutralised mock oil is shown in *Figure 7*. The hydrogenation of phenol started only when furfural was fully consumed, which is consistent with the data obtained in the acidic solution (**Error! Reference source not found.**Figure 4). However, the reaction at a pH of 6 was slower by a factor of 2.3 compared to that in acidic conditions. Moreover, no formation of C_5O and C_5OH products was observed, which shows that the selectivity in furfural hydrogenation was affected as well by the acid presence.

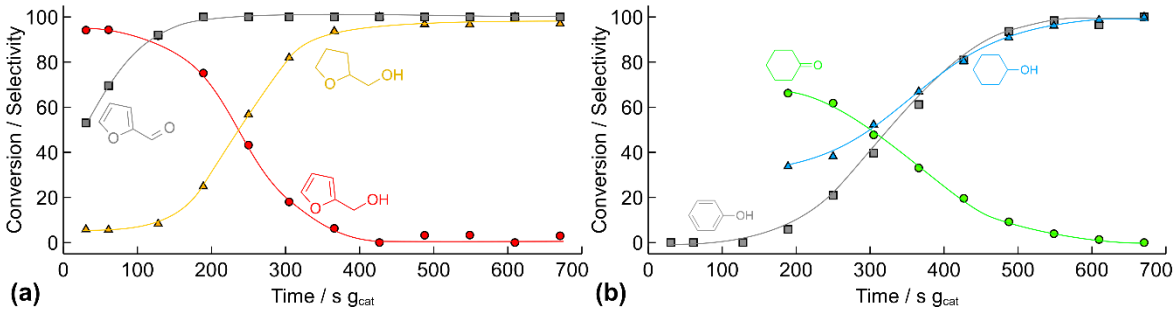

Figure 7. Product distribution in the hydrogenation of mock bio-oil (7 mM of phenol, 7 mM of furfural, and 6 mM of acetic acid in 110 mL of water). Reaction temperature: 150 °C, hydrogen pressure 50 bar. (a) furfural hydrogenation: (■) furfural conversion and selectivities towards (●) furfuryl and (▲) tetrahydrofurfuryl alcohols; (b) phenol hydrogenation: (■) phenol conversion and selectivities towards (●) cyclohexanone and (▲) cyclohexanol.

To investigate the effect of pH on the reaction rate, the mock oil was neutralized with desired amounts of the $CaCO_3$, resulting in the formation of a buffer solution. *Figure 8* shows the initial rate of hydrogenation of furfural and phenol as a function of pH. Both reaction rates remained relatively constant in the pH range from 4.5 to 6.5, while they increased substantially at a pH of 3.0. CO chemisorption data for the catalyst recovered from the reaction performed at pH of 2.8 showed very close CO capacity to that of the original catalyst. The same CO capacity shows that the accelerated hydrogenation rate in acidic medium is an occurrence caused by an intrinsic phenomenon rather than extensive de-blocking of Ru nanoparticle surface. Such a phenomenon may be explained by changing of adsorption constants near the isoelectric point of silica support (about 2.5) [70] or participation of acids in adsorption-desorption equilibria as observed for nitrite ion hydrogenation [71]. The decreased surface charge of SiO_2 support near the isoelectric point may also result in the change of an adsorption mode of reaction species. However, the scope of the study does not allow for elucidation of the mechanism involved.

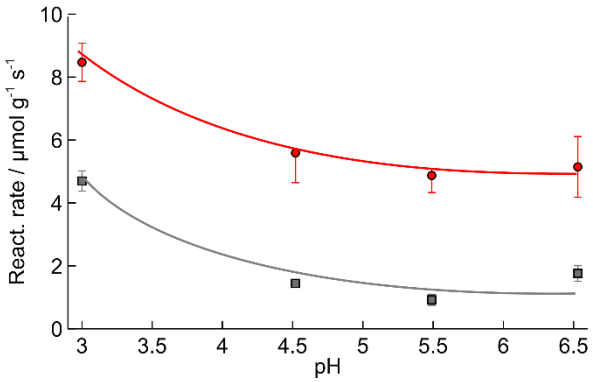

Figure 8. Initial hydrogenation rates of (●) furfural and (■) phenol in mock oil (phenol, furfural (7 mM), and acetic acid (6 mM) over the 5 wt.% Ru/SiO_2-Fe_3O_4 catalyst at 150 °C, and 50 bar hydrogen pressure).

Thus, two opposite trends are observed with changing pH values. On one hand, the catalyst activity increases at a pH value below 4.5. On the other hand, its stability decreases notably in the same range due to the dissolution of the magnetic NPs. Based on this, any pH value above 4.5 seem suitable for the repeated catalyst operation, but a higher pH value provides no additional benefits. Hence, in order to minimise the consumption of the neutralising agent and the amount of waste, the optimal pH of 4.5 was selected for the subsequent catalyst recycling study.

3.5. Catalyst recycling

Once reaction conditions were optimised, the catalytic activity was studied in several consecutive runs. In these experiments, the mock oil was neutralised with $CaCO_3$ to a pH 4.5 and 500 mg of the Ru/Fe_3O_4-SiO_2 catalyst was used. After each catalytic run, the solution was decanted, holding the catalyst with a strong (10 kg pull) FeNdB magnet, and the catalyst was dried in air at 80 °C. We have not studied alternative catalyst recycling approaches such as centrifugation or filtration because these are challenging on a larger scale due to the presence and formation of solids in the bio-oil as well as high energy and labour costs involved. The percentage of the catalyst recovery after each cycle and the reaction rates are shown in *Figure 9*.

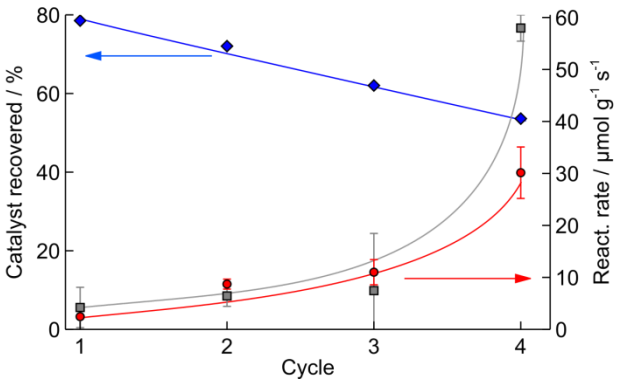

Figure 9. The fraction of the catalyst recovered and initial hydrogenation rates of (●) furfural and (■) phenol hydrogenation in consecutive catalytic cycles over the 5 wt.% Ru/SiO_2-Fe_3O_4 catalyst. The mock oil (7 mM phenol, 7 mM furfural, 6 mM acetic acid) was neutralised with a $CaCO_3$ to a pH of 4.5 at 150 ^oC and 50 bar H_2.

During these experiments, the f*raction of the catalyst recovered* steadily decreased and only 40 mg remained after the 4th cycle. After the 3rd cycle, the catalyst remaining in the solution after magnetic separation was collected via centrifugation. The mean catalyst particle size was found to be 7.2±3.4 µm (*Figure 10*a). The particles of the magnetically recovered catalyst have a mean size of 37.2±11.3 µm (*Figure 10*b), statistically indistinguishable from that in the fresh catalyst. It can be concluded that catalyst particles with a size below 15 µm cannot be recovered quickly even with a strong magnet, therefore a substantial amount of the catalyst was lost due to attrition.

It should be mentioned that the particle size did not change when the reaction was performed under magnetic stirring over the Lindlar catalyst using a stirring bar [72]. The difference is likely caused by substantially higher shear force generated by the impeller compared to a stirring bar. It is also known that the Lindlar catalyst has a higher attrition resistance as compared to that of mesoporous silica support. Huang et al. similarly observed substantial attrition of carbon-supported Pt catalysts in partial oxidation reactions [73], but optimization of the catalyst support, such as use of stronger titania, zirconia or even carbon microspheres can substantially improve attrition resistance of the catalysts [56,74,75].

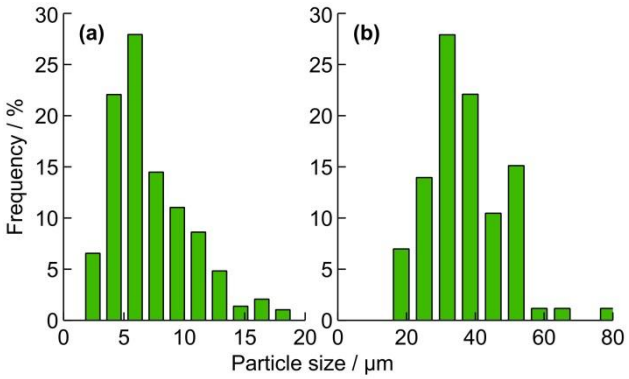

Figure 10. Particle size distribution of the 5 wt.% Ru/SiO_2-Fe_3O_4 catalyst recovered after the 3rd hydrogenation run: (a) recovered by centrifugation and (b) magnetically recovered.

Surprisingly, along with the decrease in the degree of the catalyst recovery, the reaction rate steadily increased in every subsequent hydrogenation run. To assess this effect, the magnetically recovered catalysts were studied by HR XPS to obtain further insight in this phenomena. The relative atomic concentrations of Si, Fe and Ru are listed in Table 1. The catalyst after the 4th run was not characterized by XPS because the TEM results showed a significant content of carbonaceous species rendering any further study inconclusive. Similarly, we have attempted a temperature programmed oxidation study of the recovered catalysts, but small amounts available resulted in high experimental errors and therefore, are not reported here. The XPS data show that the Fe content decreased and Ru content increased by a factor of two after the 4th catalytic run. The change in surface metal content suggests that while the catalyst particle size decreased with time due to attrition (*Figure 10*), iron oxide was removed from the catalyst increasing availability of the Ru surface to the reactants.

Table 1. Relative XPS atomic concentrations (%) of the magnetically recovered catalysts at the beginning of each hydrogenation run.

Run	Si 2p	Fe $2p_{3/2}$	Ru $3p_{3/2}$
1	75.6	11.6	12.8
2	75.2	11.9	13.0
3	75.9	9.4	14.7
4	69.1	5.5	25.4

The removal of Fe_3O_4 from the pores was unlikely caused by its dissolution at a pH of 4.5 (*Figure 6*). However, the dissolution via complexation with reaction products cannot be discarded. Therefore, an additional experiment was performed at a pH of 6.0 when the Fe_3O_4

dissolution was fully suppressed. The activity of the catalyst under such conditions increased by a factor of 1.2 in the second run, which agrees with the data obtained at the pH of 4.5. Hence, it may be concluded that the increase in catalytic activity originates from removal of Fe_3O_4 from the catalyst due to attrition as well as possible complexation with reaction products.

4. Conclusions

The magnetically recoverable composite catalyst, Ru/Fe_3O_4-SiO_2, synthesized by formation of 2 nm Ru nanoparticles in the magnetic silica that contains 5.4 nm magnetite nanoparticles located in the 6 nm silica pores, was characterized using HRTEM, XRD, and XPS. The CO chemisorption study demonstrated that only 10% of the Ru surface was accessible to the reactants indicating a significant blockage of active sites with iron oxide nanoparticles. Deoxygenation of mock pyrolysis oil containing phenol, furfural, and acetic acid (systematically studied in the 50-235 ^oC temperature range and a hydrogen pressure of 60 bar) demonstrated that phenol, furfural and furfuryl alcohol were hydrogenated into their respective derivatives suitable for fuel applications at the reaction temperature of 150 ^oC, while acetic acid required a much higher temperature. While these conditions provide minimum hydrogen and energy consumption, a noticeable catalyst dissolution was observed at a pH of 3. A pH adjustment to 6.0 decreased the rate of hydrogenation of furfural and phenol by a factor of 2. Tetrahydrofurfuryl alcohol and cyclohexanol were the main products. The difference in the reaction rate was most likely caused by different adsorption rates near the isoelectric point of the silica support. Further pH optimisation study demonstrated that the pH of 4.5 provides a reasonable compromise between the catalyst deactivation rate via dissolution and a hydrogenation reaction rate.

The degree of the catalyst magnetic recovery steadily decreased from 80% after the 1^{st} to 55 % (relative to the amount at the beginning of each run) after the 4^{th} hydrogenation run due to decreased catalyst particle size via attrition and a loss of Fe_3O_4. As a result, silica support does not seem promising for magnetically recoverable catalysts in the current reaction setup due to low attrition resistance. Hence, excellent attrition characteristics of the catalyst support such as those for titania or zirconia are required for successful magnetic recovery [56,74,75]. Contrary to expectations, the catalytic activity increased with recycling due to decreased amount of magnetite and increased accessibility of the Ru active sites.

Acknowledgement

The research leading to these results has received funding from the European Community's Seventh Framework Programme [FP7/2007-2013] under grant agreement no. 604296. We also thank the Indiana University Nanoscale Characterization Facility for access to the instrumentation as well as NSF grant #CHE-1048613 which funded Empyrean from PANalytical.

5. References

[1] N.E. Tsakoumis, M. Rønning, Ø. Borg, E. Rytter, A. Holmen, Catal. Today 154 (2010) 162–182.

[2] E. de Smit, B.M. Weckhuysen, Chem. Soc. Rev. 37 (2008) 2758–2781.

[3] A.J. Ward, D.M. Lewis, F.B. Green, Algal Res. 5 (2014) 204–214.

[4] J.J. Milledge, S. Heaven, Rev. Environ. Sci. Biotechnol. 12 (2013) 165–178.

[5] S. Czernik, A. V. Bridgwater, Energy & Fuels 18 (2004) 590–8.

[6] C.A. Mullen, A.A. Boateng, Energy and Fuels 22 (2008) 2104–2109.

[7] S. Yaman, Energy Convers. Manag. 45 (2004) 651–671.

[8] D. Mohan, C.U. Pittman, P.H. Steele, Energy & Fuesl 20 (2006) 848–889.

[9] M. Staš, J. Chudoba, D. Kubička, M. Pospíšil, Energy & Fuels 29 (2015) 3233–40.

[10] S.R.A. Kersten, W.P.M. van Swaaij, L. Lefferts, K. Seshan, in:, Catal. Renewables, Wiley-VCH Verlag GmbH & Co. KGaA, Weinheim, Germany, 2007, pp. 119–145.

[11] T. Sundqvist, A. Oasmaa, A. Koskinen, Energy & Fuels 29 (2015) 2427–2534.

[12] A. V. Bridgwater, Biomass and Bioenergy 38 (2012) 68–94.

[13] S. Xiu, A. Shahbazi, Renew. Sustain. Energy Rev. 16 (2012) 4406–14.

[14] D.C. Elliott, T.R. Hart, Energy and Fuels 23 (2009) 631–637.

[15] D.A. Ruddy, J.A. Schaidle, J.R. Ferrell III, J. Wang, L. Moens, J.E. Hensley, Green Chem. 16 (2014) 454–90.

[16] Q. Zhang, J. Chang, T. Wang, Y. Xu, Energy Convers. Manag. 48 (2007) 87–92.

[17] Y. Xiang, L. Ma, C. Lu, Q. Zhang, X. Li, Green Chem. 10 (2008) 939–43.

[18] E. Díaz, A.F. Mohedano, L. Calvo, M.A. Gilarranz, J.A. Casas, J.J. Rodríguez, Chem. Eng. J. 131 (2007) 65–71.

[19] G. Feng, P. Chen, H. Lou, Catal. Sci. Technol. 5 (2015) 2300–2304.

[20] C. Zhao, J. He, A.A. Lemonidou, X. Li, J.A. Lercher, J. Catal. 280 (2011) 8–16.

[21] H. Wan, R. V. Chaudhari, B. Subramaniam, Energy & Fuels 27 (2013) 487–93.
[22] Y. Nakagawa, K. Takada, M. Tamura, K. Tomishige, ACS Catal. 4 (2014) 2718–26.
[23] S.H. Pang, N.E. Love, J.W. Medlin, J. Phys. Chem. Lett. 5 (2014) 4110–4114.
[24] S.H. Pang, C.A. Schoenbaum, D.K. Schwartz, J. Will Medlin, ACS Catal. 4 (2014) 3123–3131.
[25] Á. O'Driscoll, T. Curtin, W.Y. Hernández, P. Van Der Voort, J.J. Leahy, Org. Process Res. Dev. 20 (2016) 1917–1929.
[26] Y. Xu, S. Qiu, J. Long, C. Wang, J. Chang, J. Tan, Q. Liu, L. Ma, T. Wang, Q. Zhang, RSC Adv. 5 (2015) 91190–91195.
[27] J. Wildschut, F.H. Mahfud, R.H. Venderbosch, H.J. Heeres, Ind. Eng. Chem. Res. 48 (2009) 10324–34.
[28] J. Wildschut, J. Arentz, C.B. Rasrendra, R.H. Venderbosch, H.J. Heeres, Environ. Prog. Sustain. Energy 28 (2009) 450–60.
[29] C. Zhao, Y. Kou, A.A. Lemonidou, X. Li, J.A. Lercher, Angew. Chemie - Int. Ed. 48 (2009) 3987–3990.
[30] Z. Tang, Q. Lu, Y. Zhang, X. Zhu, Q. Guo, Ind. Eng. Chem. Res. 48 (2009) 6923–9.
[31] A. Gutierrez, R.K. Kaila, M.L. Honkela, R. Slioor, A.O.I. Krause, Catal. Today 147 (2009) 239–46.
[32] A.H. Zacher, D.C. Elliott, M. V Olarte, D.M. Santosa, F. Preto, Energy & Fuels 28 (2014) 7510–7516.
[33] D. Wang, D. Astruc, Chem. Rev. 114 (2014) 6949–85.
[34] Z. Yinghuai, S.C. Peng, A. Emi, S. Zhenshun, Monalisa, R.A. Kemp, Adv. Synth. Catal. 349 (2007) 1917–22.
[35] V. Polshettiwar, R. Luque, A. Fihri, H. Zhu, M. Bouhrara, J.-M. Basset, Chem. Rev. 111 (2011) 3036–3075.
[36] B.R. Vaddula, A. Saha, J. Leazer, R.S. Varma, Green Chem. 14 (2012) 2133–36.
[37] O. V. Manaenkov, J.J. Mann, O. V. Kislitza, Y. Losovyj, B.D. Stein, D.G. Morgan, M. Pink, O.L. Lependina, Z.B. Shifrina, V.G. Matveeva, E.M. Sulman, L.M. Bronstein, ACS Appl. Mater. Interfaces 8 (2016) 21285–21293.
[38] S.H. Gage, B.D. Stein, L.Z. Nikoshvili, V.G. Matveeva, M.G. Sulman, E.M. Sulman, D.G. Morgan, E.Y. Yuzik-Klimova, W.E. Mahmoud, L.M. Bronstein, Langmuir 29 (2013) 466–73.
[39] Q.M. Kainz, O. Reiser, Acc. Chem. Res. 47 (2014) 667–77.

[40] L.M. Rossi, N.J.S. Costa, F.P. Silva, R. Wojcieszak, Green Chem. 16 (2014) 2906–3380.

[41] N. V. Kuchkina, D.G. Morgan, A. Kostopoulou, A. Lappas, K. Brintakis, B.S. Boris, E.Y. Yuzik-Klimova, B.D. Stein, D.I. Svergun, A. Spilotros, M.G. Sulman, L.Z. Nikoshvili, E.M. Sulman, Z.B. Shifrina, L.M. Bronstein, Chem. Mater. 26 (2014) 5654–63.

[42] H.L. Ding, Y.X. Zhang, S. Wang, J.M. Xu, S.C. Xu, G.H. Li, Chem. Mater. 24 (2012) 4572–80.

[43] R.B. Nasir Baig, R.S. Varma, ACS Sustain. Chem. Eng. 1 (2013) 805–9.

[44] R.K. Sharma, S. Dutta, S. Sharma, New J. Chem. 40 (2016) 2089–2101.

[45] J.N. Chheda, G.W. Huber, J.A. Dumesic, Angew. Chemie - Int. Ed. 46 (2007) 7164–7183.

[46] C. Zhao, Y. Kou, A.A. Lemonidou, X. Li, J.A. Lercher, Chem. Commun. 46 (2010) 412–414.

[47] P. Panagiotopoulou, N. Martin, D.G. Vlachos, J. Mol. Catal. A Chem. 392 (2014) 223–228.

[48] H. Wan, A. Vitter, R. V. Chaudhari, B. Subramaniam, J. Catal. 309 (2014) 174–184.

[49] B. Li, B. Sun, X. Qian, W. Li, Z. Wu, Z. Sun, M. Qiao, M. Duke, D. Zhao, J. Am. Chem. Soc. 135 (2013) 1181–1184.

[50] C. a Schneider, W.S. Rasband, K.W. Eliceiri, Nat. Methods 9 (2012) 671–675.

[51] R. Geyer, J. Hunold, M. Keck, P. Kraak, A. Pachulski, R. Schodel, Chemie-Ingenieur-Technik 84 (2012) 160–164.

[52] O. Hidrichsen, T. Genger, M. Muhler, Chem. Eng. Technol. 23 (2000) 956–959.

[53] Y. Wang, J. Yao, H. Li, D. Su, M. Antonietti, J. Am. Chem. Soc. 133 (2011) 2362–2365.

[54] E.-J. Shin, M.A. Keane, Ind. Eng. Chem. Res. 39 (2000) 883–892.

[55] B. Chen, U. Dingerdissen, J.G.E. Krauter, H.G.J. Lansink Rotgerink, K. Möbus, D.J. Ostgard, P. Panster, T.H. Riermeier, S. Seebald, T. Tacke, H. Trauthwein, Appl. Catal. A Gen. 280 (2005) 17–46.

[56] M.A. Tike, V. V. Mahajani, Ind. Eng. Chem. Res. 46 (2007) 3275–3282.

[57] N. Merat, C. Godawa, A. Gaset, J. Chem. Technol. Biotechnol. 48 (1990) 145–159.

[58] R. Fang, H. Liu, R. Luque, Y. Li, Green Chem. 17 (2015) 4183–8.

[59] M. Hronec, K. Fulajtarová, Catal. Commun. 24 (2012) 100–4.

[60] Y. Yang, Z. Du, Y. Huang, F. Lu, F. Wang, J. Gao, J. Xu, Green Chem. 15 (2013) 1932–40.
[61] H. Wang, J. Male, Y. Wang, ACS Catal. 3 (2013) 1047–1070.
[62] S. Sitthisa, T. Sooknoi, Y. Ma, P.B. Balbuena, D.E. Resasco, J. Catal. 277 (2011) 1–13.
[63] S. Sitthisa, D.E. Resasco, Catal. Letters 141 (2011) 784–791.
[64] W. Xu, H. Wang, X. Liu, J. Ren, Y. Wang, G. Lu, Chem. Commun. 47 (2011) 3924–6.
[65] W. Rachmady, M. Vannice, J. Catal. 192 (2000) 322–334.
[66] H. Olcay, Y. Xu, G.W. Huber, Green Chem. 16 (2014) 911–924.
[67] P.D. Vaidya, V. V Mahajani, Ind. Eng. Chem. Res. 42 (2003) 3881–3885.
[68] Y.K. Hong, W.H. Hong, Sep. Purif. Technol. 42 (2005) 151–157.
[69] G.M. Gusler, T.E. Browne, Y. Cohen, Ind. Eng. Chem. Res. 32 (1993) 2727–2735.
[70] G.A. Parks, Chem. Rev. 65 (1965) 177–198.
[71] F. Papa, I. Balint, C. Negrila, E. Olaru, I. Zgura, C. Bradu, Ind. Eng. Chem. Res. 53 (2014) 19094–19103.
[72] B. Tripathi, L. Paniwnyk, N. Cherkasov, A.O. Ibhadon, T. Lana-Villarreal, R. Gómez, Ultrason. Sonochem. 26 (2015) 445–451.
[73] Z. Huang, F. Li, B. Chen, F. Xue, Y. Yuan, G. Chen, G. Yuan, Green Chem. 13 (2011) 3414–3422.
[74] J.A. Moulijn, A.E. Van Diepen, F. Kapteijn, Appl. Catal. A Gen. 212 (2001) 3–16.
[75] M. Besson, P. Gallezot, Top. Catal. 33 (2005) 101–108.